OPEN ACCESS
IOP Publishing
Classical and Quantum Gravity
Class. Quantum Grav. **38** (2021) 185003 (16pp)
https://doi.org/10.1088/1361-6382/ac18bc

Gas cooling of test masses for future gravitational-wave observatories

Christoph Reinhardt[1,*], Alexander Franke[2], Jörn Schaffran[1], Roman Schnabel[2] and Axel Lindner[1]

[1] Deutsches Elektronen Synchrotron (DESY), 22607 Hamburg, Germany
[2] Institut für Laserphysik und Zentrum für Optische Quantentechnologien der Universität Hamburg, Hamburg, Germany

E-mail: christoph.reinhardt@desy.de

Received 18 January 2021, revised 10 June 2021
Accepted for publication 22 July 2021
Published 17 August 2021

Abstract

Recent observations made with advanced LIGO and advanced Virgo have initiated the era of gravitational-wave astronomy. The number of events detected by these '2nd generation' (2G) ground-based observatories is partially limited by noise arising from temperature-induced position fluctuations of the test mass (TM) mirror surfaces used for probing spacetime dynamics. The design of next-generation gravitational-wave observatories addresses this limitation by using cryogenically cooled test masses; current approaches for continuously removing heat (resulting from absorbed laser light) rely on heat extraction via black-body radiation or conduction through suspension fibres. As a complementing approach for extracting heat during observational runs, we investigate cooling via helium gas impinging on the TM in free molecular flow. We establish a relation between cooling power and corresponding displacement noise, based on analytical models, which we compare to numerical simulations. Applying this theoretical framework with regard to the conceptual design of the Einstein telescope (ET), we find a cooling power of 10 mW at 18 K for a gas pressure that exceeds the ET design strain noise goal by at most a factor of $\sim$3 in the signal frequency band from 3 to 11 Hz. A cooling power of 100 mW at 18 K corresponds to a gas pressure that exceeds the ET design strain noise goal by at most a factor of $\sim$11 in the band from 1 to 28 Hz.

Keywords: experimental gravitation, cryogenics, thermal noise, Einstein telescope, gas cooling

*Author to whom any correspondence should be addressed.

Original content from this work may be used under the terms of the Creative Commons Attribution 4.0 licence. Any further distribution of this work must maintain attribution to the author(s) and the title of the work, journal citation and DOI.

(Some figures may appear in colour only in the online journal)

1. Introduction

The first detection of gravitational waves by LIGO in September 2015 has unlocked a new source of information about the Universe [1]. So far, LIGO together with Virgo has observed 15 confirmed events and 35 candidate events of gravitational waves originating from mergers of two black holes, two neutron stars, as well as pairs of one black hole and one neutron star [2, 3]. In order to increase the rate and range of detections, a '3rd generation' (3G) of ground-based observatories is currently being developed [4–7]. Research targets increasing the GW signal as well as reducing the observatory's detection noise floor. The signal increases with the interferometer arm length and with the light power in the arms. Noise sources that are going to be reduced have many origins. The largest fundamental noise sources in the centre of the detector bandwidth ($\sim$100 Hz) are the quantum uncertainty in the measurement of the laser light and the thermally excited motions of the mirror surfaces. The latter are produced by thermal energy in all the different degrees of freedom of massive test mass (TM) mirrors that are suspended as pendulums under vacuum conditions. The most prominent example of thermal noise results from the Brownian motion within the dielectric high-reflectivity coatings of the mirrors.

Thermal noise is reduced if the temperature of the suspended TM mirrors is lowered. Current LIGO [8] and Virgo [9] observatories exploit mirrors at room temperature. The Japanese KAGRA [10] observatory, which began initial observations in Feb 2020 [11], exploits mirrors cooled to about 20 K. The designs of the European Einstein telescope (ET) as well as LIGO Voyager and Cosmic Explorer, the US contribution to a future 3G detector network, incorporate cryo-cooling as well. In the range from 40 Hz to 100 Hz, where thermal noise is a dominating source of noise [12, 13], a significant sensitivity improvement is expected.

Cryogenic cooling of up to $\sim$300 kg mirrors that are suspended with rather thin fibres [4, 5, 7] is a major technological challenge. The problem is how to continuously get thermal energy out of mirrors that are in vacuum and mechanically maximally decoupled from the environment, while the observatory is taking data. Heat load due to absorbed black-body radiation from the (room-temperature) kilometre-scale vacuum tubes has to be suppressed to a minimum. During operation, the test masses are constantly heated by partial absorption of laser light. Mirror substrate and coating materials need to show extremely low optical absorption in the range of a few parts per million (ppm). At the same time, the materials need to have high mechanical quality factors to channel the remaining thermal energy in narrow well-defined mechanical resonances.

In KAGRA, heat is extracted from the mirrors via suspension fibres with high thermal conductivity [14, 15]. The cooling power is provided by cryocoolers, which are connected to a separate stage of the suspension chain with flexible high-purity aluminium heat links; a dedicated vibration isolation system has been implemented to suppress the impact from cryocooler induced vibrations. For the cryogenic detector of ET, with an intended operating temperature in the range of 10 K to 20 K, a similar cooling strategy is considered [5]. Cosmic Explorer, by virtue of its higher operating temperature of 123 K, will be cooled by radiative heat transfer from the mirror to surrounding radiation shields [7]. This approach is currently being developed in the scope of LIGO Voyager [6].

Heat-exchange gas is often used for cooling down sensitive probes, which is also under investigation for GW detectors [16, 17]. Using heat-exchange gas *during* GW observations is a less obvious approach since the gas causes friction and transfers momentum to the mirror. Previously, the 1.5 tonnes bar detector Niobe used gas cooling during observation runs [18].

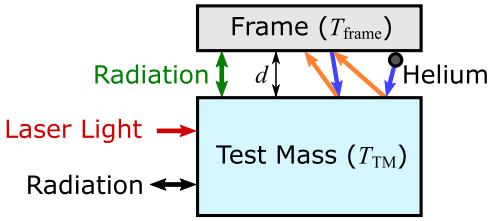

Figure 1. Schematic of a heat transfer model for gas cooling of a suspended TM. Partial absorption of laser light and thermal radiation from the environment heat the TM. The TM's temperature T_{TM} is kept constant by virtue of heat transfer to a frame, at distance d and temperature T_{frame}, via helium gas and thermal radiation. Gas cooling occurs in the free molecular flow regime (no interaction between helium atoms). Furthermore, we assume that helium atoms reach thermal equilibrium with mirror and frame. © DESY

Based on the reported parameters, we estimate the gas pressure to be above the free molecular flow regime.

Here, we investigate the potential of using helium gas in the free molecular flow regime to extract the heat imparted during observational runs in cryogenic test masses of future gravitational wave observatories. Heat transfer via conduction in suspension fibres is not included. Section 2 describes the conceptual setup. It further includes a discussion of potential challenges related to additional noise sources, arising as a consequence of injecting a significant amount of helium gas next to the mirror. Section 3 establishes, to our knowledge for the first time, the relation between gas-induced cooling power and added strain-normalized noise spectral density, based on corresponding analytical models, which are validated by comparison to numerical simulations. Our analytical models for cooling power and residual gas damping noise are also in agreement with previous publications [19, 20]. Consequences from gradually 'turning on' mutual collisions between helium atoms, thereby 'leaving' the free molecular regime, are also discussed. Section 4 presents an application of the theoretical framework described in the previous section with regard to the design of the ET. Section 5 gives concluding remarks.

2. Conceptual setup for gas cooling applied to suspended test masses

To establish models for cooling power and corresponding thermal displacement noise related to helium gas interacting with a suspended TM, we consider the setup shown in figure 1. Here, a TM suspended by thin fibres (not shown) is heated by partial absorption of laser light and thermal radiation. The imparted heat is transferred to a close-by frame, with temperature T_{frame}, by virtue of helium gas and thermal radiation, thereby keeping the TM's temperature T_{TM} constant. Thermal conduction through suspension fibres is excluded from the models presented.

The following underlying assumptions are made for the interaction between helium gas and surfaces of TM and frame: the helium gas is in the free molecular flow regime, where interactions between atoms are negligible (see subsection 3.3 for a discussion of potential consequences from gradually 'turning on' mutual collisions between helium atoms); we apply the common definition for free molecular flow based on the Knudsen number: $\mathrm{Kn} \equiv \lambda/d > 10$, with mean free path (MFP) λ and distance d between TM and frame. The MFP corresponds to the average distance travelled by atoms between successive collisions. In section 4 it is shown, that the assumption of free molecular flow leads to technically feasible values of d.

The transfer of heat between helium atoms and surfaces is specified by a corresponding accommodation coefficient α_E, which represents the fraction of incident atoms reaching thermal equilibrium with the surface [19]. Throughout this article, we consider $T_{\text{frame}} = 5$ K and $T_{\text{TM}} = 18$ K, with accommodation coefficients for helium $\alpha_E\,(5\,\text{K}) = 1.0$, $\alpha_E\,(18\,\text{K}) \equiv \alpha_{E,\text{TM}} = 0.6$ [19]. As a consequence, all gas particles emitted from the frame are assumed to be in thermal equilibrium with the frame. For the gas particles emitted from the TM, we assume that a fraction given by $\alpha_{E,\text{TM}}$ is in thermal equilibrium with the TM. The fraction given by $1 - \alpha_{E,\text{TM}}$ remains in thermal equilibrium with the frame, upon reflection from the TM. Expressing heat exchange between gas particles and surfaces in terms of the thermal accommodation coefficient is a common approach, which gives good agreement with experimental results (see, e.g. [21]). Similarly, the transfer of momentum between helium atoms and surfaces is specified by an accommodation coefficient α_M, which represents the fraction of incident atoms transferring their momentum to the surface. Here, we assume $\alpha_M\,(5\,\text{K}) = \alpha_M\,(18\,\text{K}) = 1.0$ [22, 23]. Note that unity accommodation for momentum corresponds to the worst case in terms of frictional force acting on the TM. Gas particles, which reach thermal equilibrium with or transfer their momentum to a surface, upon reflection from this surface, are said to be diffusely reflected, where the direction of re-emission from the surface is randomly distributed according to the Knudsen cosine law (see subsection 3.1 for details). The fractions of atoms $1 - \alpha_E$ and $1 - \alpha_M$, being reflected without exchange of energy or momentum with the surface, are said to be specularly reflected. We assume the duration between adsorption and desorption of an atom to be negligible.

With regard to the geometry of the frame, we assume that it fully encloses the TM's cylinder barrel (in the sense, that all lines of sight departing from the barrel reach the frame) without touching it. The underlying assumptions are consistent with a cylindrical tube concentrically surrounding a cylindrical TM at distance d. This tube would have to comprise circular baffles at its ends, e.g. with an outer diameter equal to the tube's diameter and an inner diameter marginally larger than the TM's diameter to prevent touching it. In this case, the effect on cooling power and residual gas damping noise, from not perfectly confining the gas between TM and frame, is assumed to be insignificant (see also next paragraph). With regard to a practical implementation, one may envisage a setup similar to, e.g. the advanced Virgo payload [24], with a modified reaction cage to accommodate cryogenic cooling and a baffle encapsulating the TM's barrel.

For the imperfect confinement of helium gas between TM and frame, we assume that gas particles leaking out of this region will be efficiently deflected and pumped (e.g. via cryopumping [25]), such that only an insignificant fraction of gas particles will be reflected back onto the TM. As a consequence, transfer of heat or seismic/acoustic noise to the TM from other structures inside a cryostat (see e.g. [4]) is neglected. The impact from gas damping noise, caused by helium atoms impinging on the front and backside of the TM, is considered to be insignificant, under the same assumption. An additional noise source originates from a time-varying refractive index, arising as a consequence of a fluctuating number of gas particles traversing the optical beam path inside the interferometer [26]. For helium gas leaking out of the frame, we consider this noise to be insignificant, under the assumption that the partial pressure of the helium gas will be lowered to $\sim 10^{-8}$ Pa in the vicinity of the TM. One may envisage that a corresponding cryopump could be incorporated in a helium-cooled section of the beam tube, directly adjacent to the TM cryostat. Such a cold beam tube section is described, e.g. in [4].

The analytical models and numerical simulations, presented in the following section, are based on three-dimensional gaskinetic theory; no simplification regarding the dimensionality is made. The setup studied here is simplified with regard to a possible practical implementation, as we only consider a single pendulum, representing the suspended TM, and omit other elements

of a possible payload, such as the suspended marionette (see, e.g. [4]). The motivation behind this simplification is, that only the noise acting on the suspended TM is affected by gas cooling. This approach is consistent with [5] (section 6.10.2.4), where for the suspension thermal noise, modified as a result of changing parameters of the TM's suspension fibres, with respect to the original ET design [4], just the contribution from the suspended TM is assessed.

3. Models for heat transfer and strain noise

3.1. Heat transfer model

3.1.1. General model. The cooling power acting on the TM due to the helium gas is given by

$$P_{\text{gas}} = \alpha_{E,\text{TM}} \left(\dot{Q}_{\text{out}} - \dot{Q}_{\text{in}} \right), \tag{1}$$

where $\dot{Q}_{\text{out}} \left(\dot{Q}_{\text{in}} \right)$ is the heat flux emitted (adsorbed) by the TM, in the case of unity accommodation, and $\alpha_{E,\text{TM}}$ represents the fraction of incident atoms contributing to the heat transfer (see section 2). The heat flux per surface element ΔA is calculated as the product of the flux density of emitted (adsorbed) atoms ϕ_{out} (ϕ_{in}) and their mean kinetic energy,

$$\frac{\dot{Q}_i}{\Delta A} = \phi_i \int \frac{1}{2} m_{\text{He}} v_i^2 \rho\left(v_i\right) \mathrm{d}v_i \varrho\left(\theta_i\right) \mathrm{d}\Omega_i, \tag{2}$$

with $i \in \{\text{out}, \text{in}\}$, helium mass m_{He}, speed of emitted atoms v_i, speed distribution $\rho\left(v_i\right)$, angle between the surface normal and speed vector of atom θ_i, angular distribution $\varrho\left(\theta_i\right)$, and incremental solid angle $\mathrm{d}\Omega_i = \sin\theta_i \mathrm{d}\theta_i \mathrm{d}\varphi_i$, where φ_i is the azimuthal angle. The assumptions underlying (2) are described in section 2. The corresponding speed and angular distributions are given by [27]

$$\rho\left(v_i\right) = \frac{v_i^3}{2 v_{T,i}^4} \exp\left(-\frac{v_i^2}{2 v_{T,i}^2} \right) \tag{3}$$

and

$$\varrho\left(\theta_i\right) = \frac{\cos\theta_i}{\pi}, \tag{4}$$

respectively. Here $v_{T,i} \equiv \sqrt{k_{\text{B}} T_i / m_{\text{He}}}$ is the characteristic thermal velocity, with $T_{\text{in}} = T_{\text{frame}}$ and $T_{\text{out}} = T_{\text{TM}}$. The contribution from temperature-induced position fluctuations of the TM to the relative speed between TM and gas particles is insignificant and, therefore, is not taken into account.

3.1.2. Solution for parallel plates. We consider the simple case of two parallel plates, for which (2) gives $\dot{Q}_i / \Delta A = 2 k_{\text{B}} T_i \phi_i$. This expression is obtained by substituting the three-dimensional distributions (3) and (4) into (2) and integrating v_i on $[0, \infty]$, θ_i on $\left[0, \pi/2\right]$, and φ_i on $[0, 2\pi]$. These limits of integration correspond to the entire hemisphere above the surface element. Note that the particular shape of the frame (see figure 1) is irrelevant, as long as it covers the entire hemisphere on each surface element of the TM. This is because the Knudsen cosine law (4) implies, that the number of gas particles, emitted from a surface element per solid angle into a particular direction, is independent of the orientation of the surface element with respect to the direction of emission. The reasoning behind this is, that the solid angle subtended by a surface element on the frame, with respect to a point on the TM, is proportional to

the cosine of the angle between the normal direction of this surface element and the line connecting it to the point on the TM. Based on the Knudsen cosine law, the same proportionality applies to the number of molecules emitted in this particular direction. As a result, only the total solid angle subtended by the frame matters, its shape is irrelevant, as long as its separation from the TM is compatible with the free molecular flow (see section 2). Taking into account equilibrium conditions, with equal incoming and outgoing flux $\phi_{\mathrm{out}} = \phi_{\mathrm{in}} \equiv \phi$, gives

$$\frac{\dot{Q}_i}{\Delta A} = 2k_{\mathrm{B}}T_i\phi. \tag{5}$$

As a next step, the relation between heat transfer and helium pressure is established: the pressure caused by incoming/outgoing atoms is given by the product of ϕ_i and the mean momentum along the surface normal

$$p_i = \phi_i \int m_{\mathrm{He}} v_{i\perp} \rho\left(v_i\right) \mathrm{d}v_i \varrho\left(\theta_i\right) \mathrm{d}\Omega_i, \tag{6}$$

with $v_{i\perp} = v_i \cos\theta_i$. Evaluating the integral for two parallel plates gives

$$p_i = \phi\sqrt{\frac{\pi m_{\mathrm{He}} k_{\mathrm{B}} T_i}{2}}. \tag{7}$$

Gas components coming from the frame and TM have different pressures resulting from different temperatures. This is a consequence of the assumptions detailed in section 2 (i.e. helium atoms do not interact with each other and reach thermal equilibrium with surfaces of TM and frame). By combining (1), (5), and (7) the cooling, acting on the plate at T_{TM}, can be written[3]

$$P_{\mathrm{gas}} = \alpha_{E,\mathrm{TM}}\sqrt{\frac{8k_{\mathrm{B}}}{\pi m_{\mathrm{He}} T_{\mathrm{frame}}}} p_{\mathrm{in}} \Delta A \left(T_{\mathrm{TM}} - T_{\mathrm{frame}}\right),\ \left(T_{\mathrm{TM}} > T_{\mathrm{frame}}\right), \tag{8}$$

where ΔA corresponds to the surface area of each plate. Based on the reasoning provided in the paragraph before (5), (8) also describes the heat transfer between two concentric cylinders, where ΔA corresponds to the surface area of the inner cylinder [19].

3.1.3. Maximum allowed distance between TM and frame. In the following, the maximum allowed value for the distance d between frame and TM (see figure 1) is derived. The upper bound follows from the requirement of staying in the free molecular flow regime, where $d < \lambda/10$ (see section 2). The total MFP corresponds to the average of the MFP of 'cold' atoms moving from the frame towards TM, λ_{in}, and the MFP of 'hot' ('cold') particles moving from TM towards frame, λ_{out_1} $\left(\lambda_{\mathrm{out}_2}\right)$:

$$\lambda = \frac{n_{\mathrm{in}}\lambda_{\mathrm{in}} + n_{\mathrm{out}_1}\lambda_{\mathrm{out}_1} + n_{\mathrm{out}_2}\lambda_{\mathrm{out}_2}}{n_{\mathrm{in}} + n_{\mathrm{out}_1} + n_{\mathrm{out}_2}}, \tag{9}$$

where n_{in} and n_{out_1} $\left(n_{\mathrm{out}_2}\right)$ are the number densities of incoming and outgoing 'warm' ('cold') atoms, respectively. Here, the splitting in 'warm' and 'cold' particles, moving from the TM

[3] There is an additional contribution from internal degrees of freedom, adding $\sim$0.8% of cooling power (see, e.g. [28]), which is not taken into account here.

towards the frame, is a consequence of $\alpha_{E,\mathrm{TM}} < 1$. Combining (7) with the ideal gas law $p_i = n_i k_\mathrm{B} T_i$, gives:

$$n_\mathrm{in} = \phi\sqrt{\frac{\pi m_\mathrm{He}}{2k_\mathrm{B}T_\mathrm{frame}}} \tag{10}$$

$$n_{\mathrm{out,\,1}} = \alpha_{E,\mathrm{TM}}\phi\sqrt{\frac{\pi m_\mathrm{He}}{2k_\mathrm{B}T_\mathrm{TM}}} \tag{11}$$

$$n_{\mathrm{out,\,2}} = \left(1-\alpha_{E,\mathrm{TM}}\right)\phi\sqrt{\frac{\pi m_\mathrm{He}}{2k_\mathrm{B}T_\mathrm{frame}}}. \tag{12}$$

Substituting these expressions into (9) yields

$$\lambda = \frac{\lambda_\mathrm{in} + \alpha_{E,\mathrm{TM}}\sqrt{T_\mathrm{frame}/T_\mathrm{TM}}\lambda_{\mathrm{out}_1} + \left(1-\alpha_{E,\mathrm{TM}}\right)\lambda_{\mathrm{out}_2}}{2+\alpha_{E,\mathrm{TM}}\left(\sqrt{T_\mathrm{frame}/T_\mathrm{TM}}-1\right)}. \tag{13}$$

We follow the common approach for deriving the MFP, as, for example, presented in [29]: the average distance travelled by a gas atom of 'species' $i \in \{\mathrm{in}, \mathrm{out}_1, \mathrm{out}_2\}$ between two successive collisions (i.e. the MFP) is given by $\lambda_i = \langle v_i\rangle\tau_i$, where $\langle v_i\rangle$ is the mean speed and τ_i is the average time between successive collisions. Atoms can collide either with atoms of their own species, characterized by collision time $\tau_{i,i}$, or atoms of the other species, characterized by collision times $\tau_{i,j}$ $(i \neq j)$. The total collision time for a particular species i is calculated by summing the contributing collision rates: $\tau_i^{-1} = \sum_j \tau_{i,j}^{-1}$. The rate of each collision processes is calculated by multiplying the volume of interaction per unit time by the number density of target gas particles: $\tau_{i,j}^{-1} = \pi\delta^2 n_j\langle v_{i,j}\rangle$, where δ is the kinetic diameter of a Helium atom and $\langle v_{i,j}\rangle$ is the mean relative speed between an atom of species i and an atom of species j. Combining the previous considerations yields

$$\lambda_\mathrm{in} = \frac{k_\mathrm{B}T_\mathrm{frame}\langle v_\mathrm{in}\rangle}{\pi\delta^2 p_\mathrm{in}\left[\langle v_{\mathrm{in,in}}\rangle + \alpha_{E,\mathrm{TM}}\sqrt{T_\mathrm{frame}/T_\mathrm{TM}}\langle v_{\mathrm{in,out}_1}\rangle + \left(1-\alpha_{E,\mathrm{TM}}\right)\langle v_{\mathrm{in,out}_2}\rangle\right]}, \tag{14}$$

$$\lambda_{\mathrm{out}_1} = \frac{k_\mathrm{B}T_\mathrm{TM}\langle v_{\mathrm{out}_1}\rangle}{\pi\delta^2 p_\mathrm{in}\left[\alpha_{E,\mathrm{TM}}\sqrt{T_\mathrm{frame}/T_\mathrm{TM}}\langle v_{\mathrm{out}_1,\mathrm{out}_1}\rangle + \langle v_{\mathrm{out}_1,\mathrm{in}}\rangle + \left(1-\alpha_{E,\mathrm{TM}}\right)\langle v_{\mathrm{out}_1,\mathrm{out}_2}\rangle\right]}, \tag{15}$$

$$\lambda_{\mathrm{out}_2} = \frac{k_\mathrm{B}T_\mathrm{frame}\langle v_{\mathrm{out}_2}\rangle}{\pi\delta^2 p_\mathrm{in}\left[\left(1-\alpha_{E,\mathrm{TM}}\right)\langle v_{\mathrm{out}_2,\mathrm{out}_2}\rangle + \langle v_{\mathrm{out}_2,\mathrm{in}}\rangle + \alpha_{E,\mathrm{TM}}\sqrt{T_\mathrm{frame}/T_\mathrm{TM}}\langle v_{\mathrm{out}_2,\mathrm{out}_1}\rangle\right]}. \tag{16}$$

Here, the mean speed is given by

$$\langle v_i\rangle = \sqrt{\frac{9\pi k_\mathrm{B}T_i}{8m_\mathrm{He}}}, \tag{17}$$

with $T_\mathrm{in} = T_{\mathrm{out}_2} = T_\mathrm{frame}$ and $T_{\mathrm{out}_1} = T_\mathrm{TM}$, and the mean relative speed, defined as $\langle v_{i,j}\rangle = \sqrt{\langle\left(\vec{v}_i - \vec{v}_j\right)^2\rangle} = \sqrt{\langle v_i\rangle^2 + \langle v_i\rangle^2 - 2\langle\vec{v}_i\cdot\vec{v}_j\rangle^2}$, is given by

$$\langle v_{\mathrm{in,in}}\rangle = \langle v_{\mathrm{out_2,out_2}}\rangle = \sqrt{\frac{k_{\mathrm{B}}T_{\mathrm{frame}}}{m_{\mathrm{He}}}(8-\pi)} \tag{18}$$

$$\langle v_{\mathrm{out_1,out_1}}\rangle = \sqrt{\frac{k_{\mathrm{B}}T_{\mathrm{TM}}}{m_{\mathrm{He}}}(8-\pi)} \tag{19}$$

$$\langle v_{\mathrm{out_1,out_2}}\rangle = \langle v_{\mathrm{out_2,out_1}}\rangle = \sqrt{\frac{k_{\mathrm{B}}}{m_{\mathrm{He}}}\left[4\left(T_{\mathrm{frame}}+T_{\mathrm{TM}}\right)-\pi\sqrt{T_{\mathrm{frame}}T_{\mathrm{TM}}}\right]} \tag{20}$$

$$\langle v_{\mathrm{in,out_1}}\rangle = \langle v_{\mathrm{out_1,in}}\rangle = \sqrt{\frac{k_{\mathrm{B}}}{m_{\mathrm{He}}}\left[4\left(T_{\mathrm{frame}}+T_{\mathrm{TM}}\right)+\pi\sqrt{T_{\mathrm{frame}}T_{\mathrm{TM}}}\right]} \tag{21}$$

$$\langle v_{\mathrm{in,out_2}}\rangle = \langle v_{\mathrm{out_2,in}}\rangle = \sqrt{\frac{k_{\mathrm{B}}T_{\mathrm{frame}}}{m_{\mathrm{He}}}(8+\pi)}. \tag{22}$$

The mean values are calculated based on the distribution functions given by (3) and (4).

Substituting (14) to (22) into (13) enables calculating λ based on the parameters given in section 2. The upper bound for the maximum distance between frame and TM, which is compatible with free molecular flow, is given by $d = \lambda/10$.

3.1.4. Comparison between analytical and numerical models. To validate the model presented in the previous sections, we compare it with a numerical simulation implemented in the molecular flow module of COMSOL multiphysics. We put two plates inside a closed box, which is consistent with the analytical calculation in the sense that the entire hemisphere above the warm plate is covered (see section 3.1.2). Figure 2 shows the predicted heat transfer as a function of pressure p_1 for a pair of parallel square plates, with edge length 50 cm and unity accommodation at both plates. The blue line corresponds to the analytical expression (8) and the orange circles show the values predicted by the numerical simulation. The analytical values exceed the numerical values by 0.02%. Increasing the pressure lowers the MFP, which requires a reduced separation between the plates, to be compatible with the free molecular flow regime (Kn $>$ 10). The upper x-axis shows the maximum separation between the plates still compatible with the free molecular flow, based on (13).

3.2. Strain noise model

Here, we derive the displacement noise arising from helium atoms impinging on the TM [20]. As dominant noise source we consider a single degree of freedom of the TM, corresponding to motion along the direction of the incident laser light (see figure 1) with velocity $V_{\parallel}$.

In addition to impinging gas atoms, diffusive gas flow is a potential source of noise acting on a TM in a constrained volume. The corresponding noise becomes significant if the channel limiting the flow (i.e. a gap between the TM and a nearby surface) is comparable to the dimension of the TM [30–32]. Here, we assume that gas can flow around the frame in a channel larger than TM and frame. In this case, the gap between TM and frame (see figure 1) is not limiting the flow resulting from pressure differences caused by the thermal motion of the TM along the optical axis. Therefore, we consider the noise contribution from diffusive flow negligible.

The time-averaged force per surface element ΔA of the TM's side faces is calculated as the mean value of the gas particles' flux density of momentum parallel to the TM motion

$$\frac{F_{\parallel}}{\Delta A} = \phi_{\mathrm{in}}\int m_{\mathrm{He}}v_{\mathrm{in},\parallel}\rho_{V_{\parallel}}\left(v_{\mathrm{in}}\right)\mathrm{d}v_{\mathrm{in}}\varrho\left(\theta_{\mathrm{in}}\right)\mathrm{d}\Omega_{\mathrm{in}}, \tag{23}$$

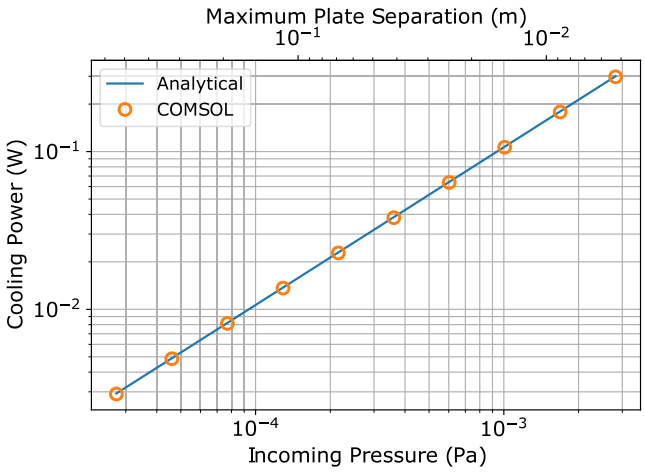

Figure 2. Heat transfer versus helium gas pressure for two parallel plates of area 50 cm × 50 cm, unity accommodation, and temperatures 5 K and 18 K, respectively. The blue line shows the analytical model (8). Values from the numerical simulation (orange circles) are lower by 0.02%. The upper x-axis indicates the separation between the plates, where shown values correspond to the upper bound compatible with free molecular flow (see main text for details). © DESY

with speed distribution

$$\rho_{V_\parallel}(v_{\text{in}}) = \frac{v_{\text{in}}^3}{2v_T^4} \exp\left[-\frac{v_{\text{in},\perp}^2 + \left(v_{\text{in},\parallel} + V_\parallel\right)^2}{2v_T^2}\right]. \tag{24}$$

Here, $v_{\text{in},\perp} = v_{\text{in}} \cos\theta_{\text{in}}\vec{e}_z$ and $v_{\text{in},\parallel} = v_{\text{in}} \sin\theta_{\text{in}}\left(\cos\varphi_{\text{in}}\vec{e}_x + \sin\varphi_{\text{in}}\vec{e}_y\right)$ are the gas particles' speed components orthogonal and parallel to $V_\parallel$, respectively, where φ_{in} is the azimuthal angle. Solving the integral gives

$$F_\parallel = -V_\parallel p_{\text{in}} \Delta A \sqrt{\frac{2m_{\text{He}}}{\pi k_{\text{B}} T_{\text{frame}}}} \equiv -V_\parallel \beta, \tag{25}$$

where the last step defines the damping coefficient β. Note that atoms re-emitted from the TM do not cause a net force. This is because emission occurs isotropically. The integral is solved analogously to the one for the heat transfer model. The details are discussed in paragraph 2 of subsection 3.1. (25) is applicable to TMs in the shape of cylinders or cubes (or any right prism) oscillating along the direction defined by a surface normal of a side face [20]. ΔA corresponds to the surface area of the cylinder's barrel or four of the cube's side faces, respectively.

Assuming the TM to represent a damped harmonic oscillator, with frictional damping force $F_\parallel$, and applying the fluctuation-dissipation theorem yields the displacement noise spectrum [33]

$$x^2(\omega) = \frac{4k_{\text{B}} T_{\text{frame}} \beta}{m_{\text{TM}}^2\left(\omega_0^2 - \omega^2\right)^2 + \beta^2\omega^2}, \tag{26}$$

where m_{TM} is the mass of the TM, $\omega_0/2\pi$ is the oscillator's resonance frequency, and $\omega/2\pi$ is the frequency.

To validate our analytical model, we set up a Monte-Carlo simulation [34]. Here, the suspended TM is modelled as a pendulum (using a small-angle approximation), with length l and displacement $z(t)$. Further assumptions are described in section 2. For each impinging atom, we assign a random timestamp and calculate the corresponding momentum transfer, based on randomly selecting four parameters: in- and outgoing speed as well as in- and outgoing angle. The underlying probability distributions for speed and angle are given by (3) and (4), respectively. The change in the TM's velocity associated with the momentum transferred by an adsorbed gas atom is given by

$$\delta V_{\parallel} = \frac{m_{\mathrm{He}}}{m_{\mathrm{TM}}} \left[v(T_{\mathrm{frame}}) \cdot \sin\, \theta_{\mathrm{in}} + v(T_{\mathrm{TM}}) \cdot \sin\, \theta_{\mathrm{out}} \right]. \tag{27}$$

The TM's trajectory is obtained based on energy conservation, giving:

$$z(t) \approx l \left(\sqrt{2\xi} + \frac{1}{24} \sqrt{2\xi}^{3} \right) \sin \left(\omega_0 t + \frac{z_0}{l} \right), \tag{28}$$

with acceleration due to gravity g, velocity added to the TM at the last hit $\delta V_{\parallel}$, TM displacement at the last collision z_0, and

$$\xi = \frac{1}{2l} \left[\frac{z_0^2}{l} + \frac{1}{g} \left(V_{\parallel} + \delta V_{\parallel} \right)^2 \right]. \tag{29}$$

The power spectral density of corresponding displacement noise is obtained by Fourier transforming the time series of TM displacements.

Figure 3 shows the simulated displacement spectral density (orange) together with the analytical model (blue, given by (26)) for a cubical toy model TM with a mass of 300 kg. The average deviation between numerical simulation and analytical model is 1%. The example illustrated here just serves as a comparison of the analytical and numerical model; the resulting displacement noise values are of no relevance whatsoever for gravitational wave detectors. With reasonable computational resources we are not able to simulate collision rates (in excess of 10^{20} s^{-1}) relevant for realistic cooling scenarios (see section 4). Therefore, in the present case, we simulate TM movement with 1.5×10^6 s^{-1}. Mirror movement is simulated for a time of 8 s.

3.3. Relation between heat transfer and strain noise

Combining (8), (25), and (26) yields the following expression (for $\omega \gg \omega_0$), directly relating the cooling power, provided by the helium atoms, to corresponding residual gas damping noise:

$$P_{\mathrm{gas}} = \alpha_{E,\mathrm{TM}} \frac{\omega^4 x^2(\omega)}{2N_{\mathrm{TM}}} \frac{m_{\mathrm{TM}}^2}{m_{\mathrm{He}}} \frac{(T_{\mathrm{TM}} - T_{\mathrm{frame}})}{T_{\mathrm{frame}}}, \tag{30}$$

where N_{TM} is the number of TMs in the detector (in all current and next generation observatories, $N_{\mathrm{TM}} = 4$). Interestingly, this expression is independent of the helium pressure p_{in} and the surface area ΔA of the TM, which is exposed to helium gas atoms. This is a consequence of the fact that for increasing/decreasing either p_{in} or ΔA, the effects from increasing/decreasing both heat flux and residual gas damping noise cancel. For a fixed amount of added mirror displacement noise, the cooling power increases with the square of the mirror mass. This corresponds to a quartic dependency on mirror diameter. Increasing the temperature of the TMs with respect to the frame leads to larger cooling power for a given amount of added noise. In that regard, increasing the accommodation coefficient is beneficial too. Furthermore, the cooling power for

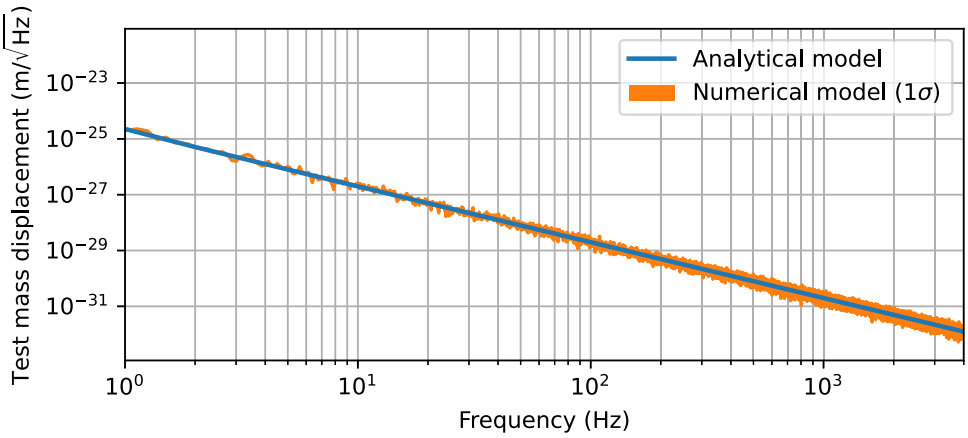

Figure 3. Residual gas damping noise from helium gas impinging on four side faces of a cubical toy model TM with mass 300 kg, suspension length 2 m, and rate of impinging helium atoms 1.5×10^6 s^{-1}. (The displacement noise values shown here are of no relevance for realistic cooling scenarios, due to a significantly lower collision rate. See main text for details). The numerical simulation (orange) is obtained by averaging seven individual noise spectra; the width corresponds to the standard deviation. The analytical model (26) (consistent with [20]) is shown in blue. The average deviation between both models is 1%. © DESY

a given amount of noise increases for lighter gas atoms and lower frame temperature. Solving (30) for the displacement noise results in an inverse proportional dependency between noise and mirror mass.

In the following, we consider the situation of two species of gas particles impinging on the TM. The first (second) species is characterized by flux density ϕ_1 (ϕ_2) and temperature $T_1 = T_{\text{frame}}$ ($T_{\text{frame}} < T_2 < T_{\text{TM}}$). For the cooling power acting on the TM follows, according to (1) and (5),

$$P_{\text{gas}} = 2k_{\text{B}}\alpha_{E,\text{TM}}\Delta A\left[\phi_1\left(T_{\text{TM}} - T_{\text{frame}}\right) + \phi_2\left(T_{\text{TM}} - T_2\right)\right]. \tag{31}$$

The corresponding frictional force, according to (25) and (7), is given by

$$F_{\parallel} = -V_{\parallel} m_{\text{He}}\Delta A\left(\phi_1 + \phi_2\right). \tag{32}$$

Based on the previous two equations, the frictional force per cooling power, $F_{\parallel}/P_{\text{gas}}$, increases for an increasing fraction of 'warm' particles, ϕ_2/ϕ_1. As a result, the damping coefficient β is greater, compared to the case with $\phi_2 = 0$. Furthermore, calculating the TM's displacement noise spectrum in this situation requires replacing T_{frame} in (26) with an average gas temperature $T > T_{\text{frame}}$. Assuming this simplified situation to be representative for the aspect of increasing the average temperature of gas particles impinging on the TM, e.g. as a consequence of gradually increasing collisions between gas particles, indicates the detrimental effects of leaving the molecular flow regime towards regimes characterized by Kn < 10.

4. Cooling power and added thermal strain noise with regard to the ET design

To assess the potential of gas cooling for future gravitational wave observatories, we examine a setup similar to the design of the cryogenic interferometer for the low-frequency ET

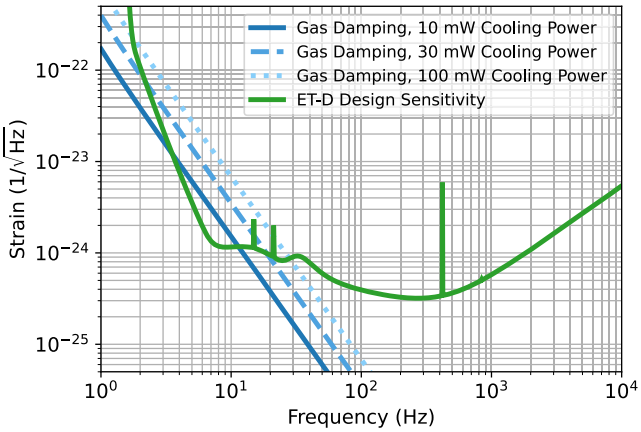

Figure 4. Residual gas damping noise from gas cooling for the ET design. The solid, dashed, and dotted blue curves show simulated strain noise spectra caused by helium atoms impinging on the four test masses, with corresponding total cooling powers per TM of 10 mW, 30 mW, and 100 mW, respectively. The green curve shows the design sensitivity of the ET. © DESY

[4, 5]. As for the ET design, we assume the interferometer to comprise four cylindrical TMs made out of silicon; each TM has a diameter $D_{\mathrm{TM}} = 45$ cm, thickness $t_{\mathrm{TM}} = 57$ cm, and mass $m_{\mathrm{TM}} = 211$ kg. The expected heat load from absorbed laser light and thermal radiation is $\sim$100 mW, which, according to the baseline design, is fully extracted by conduction through the TM's silicon suspension fibres. In the case of gas cooling as complementing cooling strategy, the imparted heat is transferred to a frame surrounding the barrel of a TM (see section 2). Here, we assume TM and frame temperatures of $T_{\mathrm{TM}} = 18$ K and $T_{\mathrm{frame}} = 5$ K, respectively. At this value for T_{TM}, the coefficient of thermal expansion for silicon vanishes, thereby eliminating noise from thermoelastic damping. The cooling power provided by the helium gas is calculated according to (8), with $\Delta A = A_{\mathrm{barrel}} = \pi D_{\mathrm{TM}} t_{\mathrm{TM}}$. The contribution from radiation is calculated based on the Stefan–Boltzmann law $\sigma\left(\varepsilon_{\mathrm{barrel}} A_{\mathrm{barrel}} + \varepsilon_{\mathrm{face}} \pi D_{\mathrm{TM}}^2/2\right)\left(T_{\mathrm{TM}}^4 - T_{\mathrm{frame}}^4\right)$, with Stefan–Boltzmann constant σ, emissivity of the TM's barrel $\varepsilon_{\mathrm{barrel}} = 0.9$, and emissivity of the TM's front and backside $\varepsilon_{\mathrm{TM}} = 0.6$ [6]. Here, the contribution from the TM's barrel is linear in D_{TM} and the contribution from the TM's side is quadratic in D_{TM}. For the given parameters, a radiative cooling power of 5 mW is predicted.

Figure 4 shows the noise associated with gas cooling together with the sensitivity of the ET design (ET-D) [4, 5]. All values are given in terms of strain, which is defined as $x(\omega)/L$, where L is the distance between the two TMs in an arm of the interferometer. Here, we assume the value of the ET design: $L = 10$ km [4, 5]. The expected heat load on each TM is 100 mW, according to [5], section 6.10.2.4. An optimistic estimate considers just the absorption in the optical coating, contributing 18 mW (i.e. 1 ppm absorption of 18 kW circulating power, according to [5], section 6.11.2), and an additional contribution of $\sim$10 mW from thermal radiation (see [4], section 3.9.2), resulting in a corresponding heat load of $\sim$30 mW. This estimate assumes optical absorption in the substrate to be negligible. For 10 mW of total cooling power (e.g. a 10% contribution to extract the expected heat load), with equal contributions from helium gas and radiation, the noise from cooling (solid blue line) exceeds the ET-D sensitivity (green) by at most a factor of 2.3 in a narrow frequency band from 3 to 11 Hz. The corresponding helium pressure is 2×10^{-5} Pa, which imposes the bound $d < 66$ cm on the

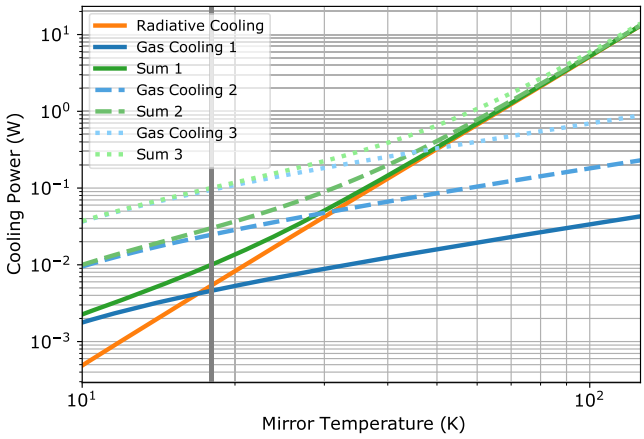

Figure 5. Cooling power versus TM temperature for the ET design. The solid dashed, and dotted blue curves show the cooling power provided by helium gas according to (30), where the corresponding strain noise is shown in figure 4 by curves of the same formatting. The orange line shows the contribution from radiative heat transfer (details provided in the main text). The solid dashed, and dotted green curves show the sum of contributions from cooling by gas and radiation. The vertical grey line indicates a temperature of the TM mirrors of 18 K. © DESY

distance between TM and frame, for compatibility with free molecular flow. Extracting a heat load of 30 mW (100 mW) requires 25 mW (95 mW) of cooling power provided by the helium gas. The corresponding helium pressure is 12×10^{-5} Pa $\left(46 \times 10^{-5}\,\text{Pa}\right)$, which imposes the bound $d < 12$ cm $(d < 3$ cm) for compatibility with free molecular flow. The resulting noise, shown by the dashed (dotted) blue line exceeds the ET-D sensitivity by at most a factor of 5.3 (10.3) in the frequency band from 2 Hz (1 Hz) to 19 Hz (28 Hz). These results indicate that, for the given detector configuration, increasing the cooling power comes at the cost of simultaneously increasing the residual gas damping noise. Getting 10 mW, 30 mW, or 100 mW of cooling power with a maximum added noise comparable to the ET-D sensitivity (represented by the solid green curve in figure 4) requires $m_{\text{TM}} \sim 500$ kg, $m_{\text{TM}} \sim 1100$ kg, or $m_{\text{TM}} \sim 2200$ kg, respectively.

Figure 5 shows the total cooling power and its contributors versus TM temperature. The solid dashed, and dotted blue curves represent the contribution from helium gas, where the corresponding noise is shown by the curves of similar formatting in figure 4. For helium pressures corresponding to 10 mW, 30 mW, or 100 mW of cooling power at $T_{\text{TM}} = 18$ K, radiative cooling dominates over gas cooling for $T_{\text{TM}} > 17$ K, $T_{\text{TM}} > 31$ K, or $T_{\text{TM}} > 50$ K, respectively.

5. Conclusion

Based on a conceptual setup of a suspended TM mirror in future GW observatories, we have established a relation between gas-induced cooling power and corresponding added observatory strain noise. In this process, we have developed analytical models for cooling power and noise, which we compared to numerical simulations, finding excellent agreement within 1% for both heat transfer and noise model; our noise model is also consistent with the one presented in [20]. For the considered setup, where heat is transferred between the mirror's cylinder barrel

and a close-by frame, we have shown that the gas-induced cooling power, for a fixed amount of added mirror displacement noise, increases with the square of the mirror mass. This corresponds to a quartic dependency on mirror diameter for gas cooling. For comparison, the mirror's radiative cooling power is a sum of contributions from surfaces of cylinder barrel and sides, with linear and quadratic dependency on the mirror's diameter, respectively. Note that increasing mirror diameter and mass also suppresses other noise contributors and is overall beneficial for the sensitivity of gravitational wave detectors [4, 5]. We also have applied our theoretical framework with regard to the ET design, assuming a mirror temperature of 18 K and mirror masses of 211 kg: A gas cooling power of 10 mW introduces additional noise exceeding the ET design sensitivity by a factor $\sim$3 in a frequency band from 3 to 11 Hz. A gas cooling power of 100 mW results in additional noise exceeding the ET design sensitivity by a factor $\sim$11 in a frequency band from 1 to 28 Hz. We have pointed out that hypothetically increasing the mirror mass by a factor of 3 and 11, for a cooling power of 10 mW and 100 mW, respectively, reduces the gas-induced strain noise to a level, which is at most comparable to the ET design sensitivity. This illustrates the inverse proportionality between strain noise and mirror mass for a fixed gas cooling rate. The considered cooling powers comprise an estimated 5 mW from radiative cooling, which corresponds to 5% of the expected heat load. With regard to the current baseline cooling concept for the ET project, we have pointed out the potential benefit of additional cooling power, provided by gas cooling, and resulting limitations in form of added observatory strain noise. Gas cooling should be considered as an additional resource in combination with the currently-used conductive cooling when designing third generation detectors. The uncertainty in the accommodation coefficient makes an experimental test of the proposed cooling approach desirable.

Acknowledgments

We thank Sandy Croatto, Michael Hartman, and Mikhail Korobko for helpful discussions. This work was supported and partly financed (AF) by the DFG under Germany's Excellence Strategy EXC 2121 'Quantum Universe'-390833306.

Data availability statement

The data that support the findings of this study are available upon reasonable request from the authors.

ORCID iDs

Christoph Reinhardt https://orcid.org/0000-0002-5976-4430
Alexander Franke https://orcid.org/0000-0002-4843-1112
Roman Schnabel https://orcid.org/0000-0003-2896-4218

References

[1] Abbott B P *et al* 2016 Observation of gravitational waves from a binary black hole merger *Phys. Rev. Lett.* **116** 061102

[2] Abbott B P *et al* 2019 Gwtc-1: a gravitational-wave transient catalog of compact binary mergers observed by ligo and virgo during the first and second observing runs *Phys. Rev.* X **9** 031040
[3] Abbott R *et al* 2020 Gwtc-2: compact binary coalescences observed by Ligo and Virgo during the first half of the third observing run (arXiv:2010.14527)
[4] Abernathy M *et al* 2011 Einstein gravitational wave telescope conceptual design study *Technical Report No. ET-0106C-10*
[5] ET Steering Committee Editorial Team 2020 *Einstein Telescope Design Report Update 2020*
[6] Adhikari R X *et al* 2020 A cryogenic silicon interferometer for gravitational-wave detection *Class. Quantum Grav.* **37** 165003
[7] Reitze D *et al* 2019 Cosmic explorer: the us contribution to gravitational-wave astronomy beyond Ligo (arXiv:1907.04833)
[8] Aasi J *et al* 2015 Advanced Ligo *Class. Quantum Grav.* **32** 074001
[9] Acernese F *et al* 2014 Advanced Virgo: a second-generation interferometric gravitational wave detector *Class. Quantum Grav.* **32** 024001
[10] Somiya K 2012 Detector configuration of kagra – the Japanese cryogenic gravitational-wave detector *Class. Quantum Grav.* **29** 124007
[11] Akutsu T *et al* 2020 Overview of kagra: detector design and construction history (arXiv:2005.05574)
[12] Buikema A *et al* 2020 Sensitivity and performance of the advanced ligo detectors in the third observing run *Phys. Rev.* D **102** 062003
[13] Acernese F *et al* 2020 Advanced Virgo status *J. Phys.: Conf. Ser.* **1342** 012010
[14] Akutsu T *et al* 2019 First cryogenic test operation of underground km-scale gravitational-wave observatory kagra *Class. Quantum Grav.* **36** 165008
[15] Ushiba T *et al* 2021 Cryogenic suspension design for a kilometer-scale gravitational-wave detector *Class. Quantum Grav.* **38** 085013
[16] Shapiro B *et al* 2017 Cryogenically cooled ultra low vibration silicon mirrors for gravitational wave observatories *Cryogenics* **81** 83–92
[17] Bonilla E and Lantz B 2019 Improving the cool-down times for third generation gravitational wave observatories (Lvc) LIGO document, LIGO-G1900526-V1 https://dcc.ligo.org/LIGO-G1900526/public
[18] Tobar M E, Blair D G, Ivanov E N, Van Kann F, Linthorne N P, Turner P J and Heng I S 1995 The university of western Australia? s resonant-bar gravitational wave experiment *Aust. J. Phys.* **48** 1007–26
[19] Corruccini R J 1959 Gaseous heat conduction at low pressures and temperatures *Vacuum* **7** 19–29
[20] Cavalleri A, Ciani G, Dolesi R, Hueller M, Nicolodi D, Tombolato D, Vitale S, Wass P J and Weber W J 2010 Gas damping force noise on a macroscopic test body in an infinite gas reservoir *Phys. Lett.* A **374** 3365–9
[21] Trott W M, Castañeda J N, Torczynski J R, Gallis M A and Rader D J 2011 An experimental assembly for precise measurement of thermal accommodation coefficients *Rev. Sci. Instrum.* **82** 035120
[22] Agrawal A and Prabhu S V 2008 Survey on measurement of tangential momentum accommodation coefficient *J. Vac. Sci. Technol.* A **26** 634–45
[23] Cao B-Y, Chen M and Guo Z-Y 2005 Temperature dependence of the tangential momentum accommodation coefficient for gases *Appl. Phys. Lett.* **86** 091905
[24] Naticchioni L *et al* (Virgo Collaboration) 2018 The payloads of advanced virgo: current status and upgrades *J. Phys.: Conf. Ser.* **957** 012002
[25] Gil W, Bonn J, Bornschein B, Gehring R, Kazachenko O, Kleinfeller J and Putselyk S 2009 The cryogenic pumping section of the katrin experiment *IEEE Trans. Appl. Supercond.* **20** 316–9
[26] Zucker M E and Whitcomb S E 1996 Measurement of optical path fluctuations due to residual gas in the ligo 40 meter interferometer *Proc. 7th Marcel Grossman Meeting on Recent Developments in Theoretical and Experimental General Relativity, Gravitation, and Relativistic Field Theories* pp 1434–6
[27] Celestini F and Mortessagne F 2008 Cosine law at the atomic scale: toward realistic simulations of Knudsen diffusion *Phys. Rev.* E **77** 021202
[28] Gombosi T I and Gombosi A 1994 *Gaskinetic Theory* (Cambridge: Cambridge University Press) ch 7.2.3 p 9
[29] James J 1982 *An Introduction to the Kinetic Theory of Gases* (*Cambridge Science Classics*) (Cambridge: Cambridge University Press)

[30] Stephan S 2010 Comparison of squeeze film damping simulations for the advanced Ligo geometry LIGO Document, LIGO-T1000101-V1 http://ligo.caltech.edu/docs
[31] Cavalleri A *et al* 2009 Increased brownian force noise from molecular impacts in a constrained volume *Phys. Rev. Lett.* **103** 140601
[32] Weiss R 2009 Gas damping of the final stage in the advanced Ligo suspensions LIGO document, LIGO-T0900509-v1 https://dcc.ligo.org/LIGO-T0900509/public
[33] Saulson P R 1990 Thermal noise in mechanical experiments *Phys. Rev.* D **42** 2437
[34] Evans M, Fritschel P and Weiss R (LIGO Scientific Collaboration) 2011 Gas damping Monte Carlo *Technical Report LIGO-T0900582*